frontiers | Frontiers in Earth Science

TYPE Original Research
PUBLISHED 04 July 2024
DOI 10.3389/feart.2024.1416308

Check for updates

OPEN ACCESS

EDITED BY
Shida Chen,
China University of Geosciences, China

REVIEWED BY
Yanjun Meng,
Taiyuan University of Technology, China
Jiang Han,
Yanshan University, China
Ang Liu,
The Pennsylvania State University (PSU), United States

*CORRESPONDENCE
Yan Zhang,
geozhangyan@outlook.com

RECEIVED 12 April 2024
ACCEPTED 11 June 2024
PUBLISHED 04 July 2024

CITATION
Zhang Y and Liu J (2024), *In-situ* geological conditions and their controls on permeability of coalbed methane reservoirs in the eastern Ordos Basin.
Front. Earth Sci. 12:1416308.
doi: 10.3389/feart.2024.1416308

COPYRIGHT
© 2024 Zhang and Liu. This is an open-access article distributed under the terms of the Creative Commons Attribution License (CC BY). The use, distribution or reproduction in other forums is permitted, provided the original author(s) and the copyright owner(s) are credited and that the original publication in this journal is cited, in accordance with accepted academic practice. No use, distribution or reproduction is permitted which does not comply with these terms.

In-situ geological conditions and their controls on permeability of coalbed methane reservoirs in the eastern Ordos Basin

Yan Zhang* and Jincheng Liu

[1]Research Institute of Petroleum Exploration and Development, PetroChina, Beijing, China

The eastern Ordos Basin plays an important role in China's coalbed methane (CBM) industry, boasting considerable CBM resources and pronounced reservoir heterogeneity, making it an ideal site for comparative research on deep and shallow CBM geology. In order to dissect the fundamental reasons for significant differences in production capacity between blocks and promote mutual learning from successful development experiences, this paper conducts a systematical study on the distribution characteristics of *in-situ* geological conditions of CBM reservoirs based on extensive well-testing data. Additionally, through coal permeability sensitivity experiments on coal samples with various $R_{o,\ max}$ values, burial depths, and initial permeabilities, this study explores the change law of permeability during the process of CBM extraction. The results indicate that as the burial depth of coal seam increases, so do the temperature, pressure, and stress. Moreover, the distribution of geothermal gradient, reservoir pressure gradient, horizontal stress gradient, and lateral pressure coefficient tends to converge with increasing burial depth, with a turning depth typically between 1,000 and 1,500 m. Coal seams below 1,500 m generally exhibit a normal-fault type stress field with normal-overpressure. *In-situ* permeability decreases with depth, but the permeability in deep stress relief zones can be maintained at a relatively high level. A lower initial permeability corresponds to a smaller stress sensitivity coefficient and reduced temperature sensitivity effects, resulting in slower permeability damage during CBM extraction. However, when the reservoir pressure drops to depletion pressure, the maximum damage rate of permeability increases significantly, underscoring the importance of reservoir reconstruction in deep CBM development. This study provides a theoretical basis for selecting favorable areas for CBM exploration and development, as well as for designing efficient development plans in practice.

KEYWORDS

eastern Ordos Basin, CBM reservoir, *in-situ* geological conditions, depth effect, permeability sensitivity

1 Introduction

Report on China oil and gas resource exploration and development in 2020 (Ministry of Natural Resources, PRC, 2020) shows that, as of the end of 2020, China's proven geological reserves of CBM were 7259.11 × 10^8 m^3, and the cumulative production of CBM reached 288.66×10^8 m^3, mainly from the Qinshui Basin and the eastern Ordos Basin. The development of shallow CBM in the Baode, Sanjiao, Liulin, and Hancheng blocks in the eastern Ordos Basin is relatively mature. In recent years, exploration and development work has gradually expanded to deep blocks such as Yanchuannan, Linxing, Daning-Jixian, Shenfu, and Shilou (Yang et al., 2022). However, the complexity of the geological environment of CBM reservoirs has caused significant differences in the development effects between blocks (Yan et al., 2021).

The *in-situ* geological environment of CBM reservoirs is mainly reflected in three aspects: stress, temperature, and fluid pressure. Based on the measurement data of reservoir stress in different regions, previous researchers have recognized that the lateral pressure coefficient (average horizontal principal stress/vertical stress) of the formation exhibits a clear regularity in the vertical direction (Brown and Hock, 1980; Zhao et al., 2007; Kang et al., 2009; Qin et al., 2012; Chen et al., 2018a; Kang et al., 2019; Fu et al., 2020). The stress field of shallow CBM reservoirs is mainly horizontal stress. Due to its proximity to the surface and high degree of structural development, the measurement results of stress are scattered, and the distribution range of lateral pressure coefficients is large. However, in deep CBM reservoirs, the principal stress gradually transitions to the vertical direction, and the lateral pressure coefficient continuously decreases and converges. As the burial depth increases, the pressure of CBM reservoirs generally shows an increasing trend (Liu et al., 2012; Milkov and Etiope, 2018; Fu et al., 2020). On the one hand, increasing depth and stress can lead to a decrease in pore volume compression, but due to a certain fluid content, it can cause an increase in reservoir fluid pressure (Zhong, 2003). On the other hand, the pressure of the reservoir is also related to the mineralization degree of groundwater. Generally, the higher the mineralization degree, the greater the static water pressure gradient, and the greater the pressure of the CBM reservoir (Wu et al., 2007). The difference in groundwater head height can also cause changes in reservoir pressure and its pressure gradient by controlling the direction of water flow. Generally, the lower the head height, the smaller the pressure gradient, and the lower the reservoir pressure (Zhang and Tang, 2001; Jing, 2012). Qin et al. (2012) analyzed the fluid dynamics characteristics of the Shanxi and Taiyuan formations in the eastern part of the Ordos Basin and found that due to differences in rock permeability, the pressure system of deep CBM reservoirs is significantly controlled by sedimentary frameworks, often having relatively independent gas and pressure systems. At the same time, coal seam temperature is widely believed to have a linear positive correlation with burial depth (Liu, 2006; Wu et al., 2013; Zhao et al., 2019; Fu et al., 2020). However, some scholars have pointed out that the relationship between ground temperature and burial depth is much more complex than a linear relationship (Chapman et al., 1984). In addition to burial depth, multiple factors can affect reservoir temperature (Xiao et al., 2009), and ground temperature cannot be calculated solely by depth (Gan et al., 2019).

As a reservoir mainly composed of organic matter, coal seams are more sensitive to stress, pressure, and temperature than conventional "inorganic" reservoirs. Under the influence of high stress and formation temperature, the geological conditions of deep CBM reservoirs are more complex (Chen et al., 2018b; Salmachi et al., 2021). The permeability of coal seams is an important indicator for the optimization of CBM exploration and development areas, and the extremely low permeability of deep coal seams is currently the key obstacle to the exploitation and utilization of deep CBM resources (Ranathunga et al., 2014). The permeability of CBM reservoirs is influenced by multiple factors such as stress, reservoir pressure, and temperature (Li et al., 2012; Song et al., 2013). Among them, the tectonic stress field is the dominant factor in the permeability of coal seams. The ancient tectonic stress field determines the formation and development of fractures, while the current tectonic stress field determines the closure degree of fractures (Bell, 2006; Chatterjee et al., 2019). Some scholars have found that with the increase of effective stress, the permeability of coal seams decreases exponentially (Dabbous et al., 1974; Karacan and Okandan, 2001). However, some scholars hold different views and explain the overall law of dynamic changes in permeability. They believe that during the elastic-plastic strain stage, as stress increases, fresh microcracks will continue to develop in coal, and permeability will continue to improve; The closer to the peak stress, the greater the generation of microcracks, which are interconnected and have a sharp increase in permeability; After reaching the peak strength, the coal rock loses its maximum bearing capacity, and the permeability continues to increase, but the growth rate slows down; When the elastic deformation reaches a certain level, the permeability reaches its minimum value, and the maximum permeability occurs during the softening or plastic flow stage (Harpalani and Chen, 1992; Li et al., 2001; Wang et al., 2018). It can be seen that the *in-situ* stress control effect of CBM reservoir permeability characteristics still needs further research, but it can be affirmed that as the burial depth increases, the anisotropy of stress state will gradually increase its impact on coal seam permeability, which needs to be paid attention to (Paul and Chatterjee, 2011; Reisabadi et al., 2021).

The effect of temperature on coal seam permeability is also a focus of attention for scholars. The control effect of coal seam temperature on permeability is mainly reflected in two aspects: on the one hand, as the temperature increases, the coal body continuously expands, the methane migration channels decrease, and the gas phase permeability also continuously decreases; On the other hand, methane viscosity decreases with increasing temperature, flow resistance decreases, and gas-phase permeability increases accordingly (Cheng et al., 1998; Yang et al., 2005a; Pan and Connell, 2011; Liu et al., 2021). Some scholars believe that temperature has a certain negative effect on permeability as a whole, but this negative effect is only more obvious when the stress level is low, and gradually weakens with increasing stress (Yang and Zhang, 2008; Gao, 2019). Moreover, the temperature sensitivity of permeability in CBM reservoirs of different coal ranks is different and generally weakens with increasing coal ranks (Wu et al., 2017).

The eastern Ordos Basin is a hot area for CBM exploration and development, with diverse geological conditions, providing an excellent platform for comparative research. At present, due

to the lack of core sampling and testing data of deep wells, the study of differences between blocks is still chaotic, and the permeability controlling mechanism of CBM reservoirs is not yet clear, making it difficult to learn from successful development experiences. Based on the analysis of drilling and well testing data during the exploration and development of CBM, this study determines the distribution characteristics of *in-situ* temperature, pressure, stress, and permeability, as well as explores the stress/temperature sensitivity and depth effect of permeability through coal permeability sensitivity experiments.

2 Geological setting

The Ordos Basin is located in the western part of the North China Plate in China and is a typical large-scale superimposed basin with stable craton margins. The overall shape is rectangular with a north-south distribution, and the terrain and structural complexity continuously decrease from the basin edge to the inside of the basin. The entire basin is composed of six primary tectonic units (Figure 1A). The eastern Ordos Basin is mainly located in the Jinxi Flexural Belt (Wang et al., 2010), transitioning to the Yishan Slope on the west side, and bordered by the Lishi Fault on the east, adjacent to the Shanxi Platform. Spanning 500 km from north to south and with a width of 40–60 km from east to west, the basin covers an area of 2.7×10^4 km^2. It exhibits a monocline structure with a high eastern side and a low western side, with a dip angle of 2°–3°. The CBM work area in eastern Ordos Basin is divided into ten major blocks from north to south based on the structural pattern, namely,: Baode, Shenfu, Linxing (East/Central/West), North Sanjiao, Sanjiao, Liulin, Shilou (North/West/South), Daning-Jixian, Yanchuannan, and Hancheng blocks (Figure 1B).

The Carboniferous-Permian coal-bearing strata in the eastern Ordos Basin have undergone four tectonic changes since sedimentation, including the Hercynian, Indosinian, Yanshanian, and Himalayan periods (Li and Zhang, 2020) (Figure 1C). In the Hercynian period, the North China ancient plate entered a slow subsidence stage and began to receive sedimentation. The coal-bearing strata of the Carboniferous-Permian marine-continental transition phase was formed as a result (310–280 Ma). By the end of the Late Permian, the burial depth of the top surface of the Taiyuan Formation increased from north to south, ranging from 200 to 1,200 m. From the early Triassic to the end of the late Triassic, the subsidence rate of the strata increased sharply, and the subsidence depth of the strata showed a nearly linear increase. The subsidence rate was relatively stable, and the ancient temperature also rapidly increased, leading to differences in the degree of coal metamorphism. In the Indosinian movement, the strata experienced slight uplift and subsidence fluctuations. By the end of the Middle Jurassic, the top surface of the Taiyuan Formation reached its maximum burial depth, distributed from north to south within the range of 1,600–3,600 m. Due to differences in burial depth, the temperature difference between the north and south regions reached 80°C (Li and Zhang, 2020). The Yanshan Movement has significant implications for the evolution of tectonic morphology in the eastern margin. At the end of the Early Cretaceous, the crust rapidly uplifted, ending the sedimentation of the depression basin. The overlying strata suffered from strong weathering and erosion, continuous thinning, and greater uplift at the edge of the basin. During the Himalayan period, the subsidence and uplift amplitude of the coal seam are relatively small. According to the lithological combination, the Carboniferous Permian strata in the eastern Ordos Basin were divided from bottom to top into the Benxi Formation, Taiyuan Formation, Shanxi Formation, Lower Shihezi Formation, and Upper Shihezi Formation with multiple sets of coal seams developed in Taiyuan and Shanxi formations (Chen, 1989) (Figure 2). The coalification process in the eastern Ordos Basin is mainly characterized by deep metamorphism, except for the Zijinshan area, and the degree of coal metamorphism is increasing from north to south as a whole (Li and Zhang, 2020).

3 Materials and methods

3.1 *In-situ* parameters acquisition

In-situ parameters including temperature, pressure, stress and permeability are mainly derived from injection/pressure drop well testing reports. The data obtained from hydraulic fracturing in Central Linxing Block is limited, which is not enough to characterize the difference in regional stress fields. Therefore, log data are used to inversion the *in-situ* stress in the Central Linxing Block. For detailed steps of the two methods, please refer to Pu et al. (2022).

3.2 Coal permeability sensitivity experiment

Eleven coal samples with various $R_{o,\,max}$ values, burial depths, and initial permeabilities were selected from different blocks of the eastern Ordos Basin, including Central Linxing, Liulin, Yanchuannan, and Hancheng, for comparative analysis of the stress and temperature sensitivity of coal permeability. The basic information of the coal samples is shown in Table 1. The instrument used in this experiment is the AP-608 automated permeameter-porosimeter produced by CoreTest in the United States. Permeability measurement is based on the unsteady-state pressure decay method. The confining pressure is loaded through Hassler type/hydrostatic pressure, with a variation range of 500–9,500 psi, which is 3.45–65.5 MPa. To measure permeability, a pressure pulse within the range of 100–250 psi (0.67–1.72 MPa) is sent through the sample. The instrument has a pressure sensor accuracy of ±0.1%, and the measurement range for permeability is 0.001–10000 mD. The testing gas source uses high-purity helium gas.

In order to investigate the impact of stress on coal permeability, we employed changes in net confining pressure to simulate variations in effective stress within the coal seam. Subsequently, the coal permeability was measured in relation to changes in net confining pressure, and the relationship between permeability and effective stress was analyzed. The pressure of the CBM reservoirs in the Liulin and Hancheng districts is within the range of 2.2–9.9 MPa and 4.1–11.9 MPa, respectively, with a maximum value not exceeding 12 MPa. In order to better reflect the dynamic change process of coal seam permeability with the increase of effective

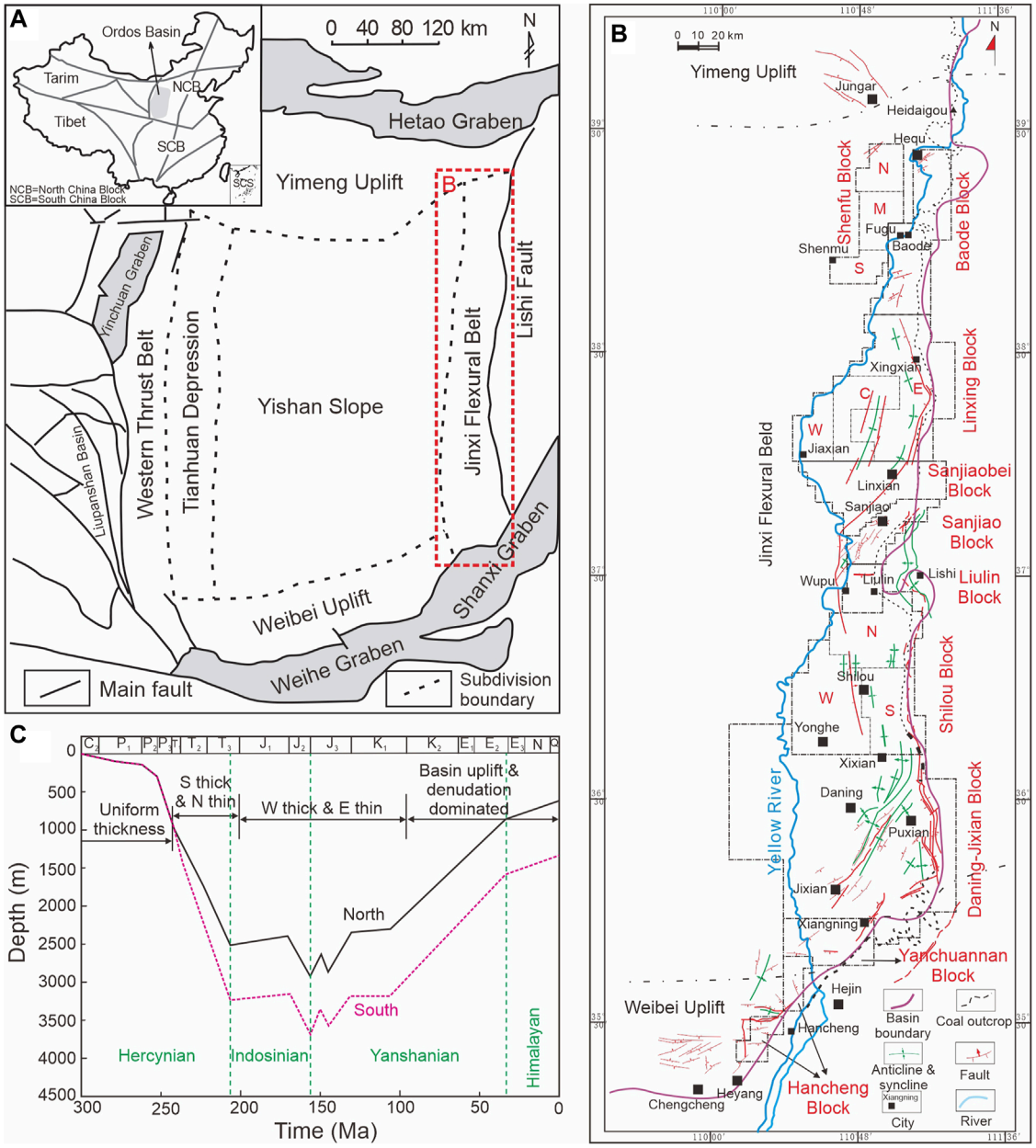

FIGURE 1
Geological map of the eastern Ordos Basin **(A)** Tectonic location; **(B)** Schematic map of CBM block zoning; **(C)** Schematic diagram of differential tectonic evolution (modified from Li and Zhang (2020)).

stress in the process of CBM drainage in the Liulin and Hancheng blocks, the experimental confining pressure range is 3.45–12 MPa, and a total of 4 pressure points of 3.45, 6, 9, and 12 MPa are set. For the Linxing and Yanchuannan samples with deeper burial depth, due to their reservoir pressure reaching up to 21.22 MPa, the testing pressure range is set to 3.45–25 MPa, and a total of 6 pressure points of 3.45, 5, 10, 15, 20, and 25 MPa are set. In addition, due to the temperature of deep CBM reservoirs reaching 60°C, exploring the effect of temperature on the permeability of CBM reservoirs is also of great significance. Therefore, in addition to the above tests conducted at room temperature (20°C), temperature sensitivity tests were conducted on the Lin 1 and Yan 1 samples, with two additional experimental control groups of 40°C and 60°C added.

4 Results and discussion

4.1 *In-situ* geological conditions

4.1.1 Geotemperature field

The temperature conditions of coal seams directly affect the adsorption, desorption, and production processes of CBM. Therefore, revealing the *in-situ* temperature conditions of the coal

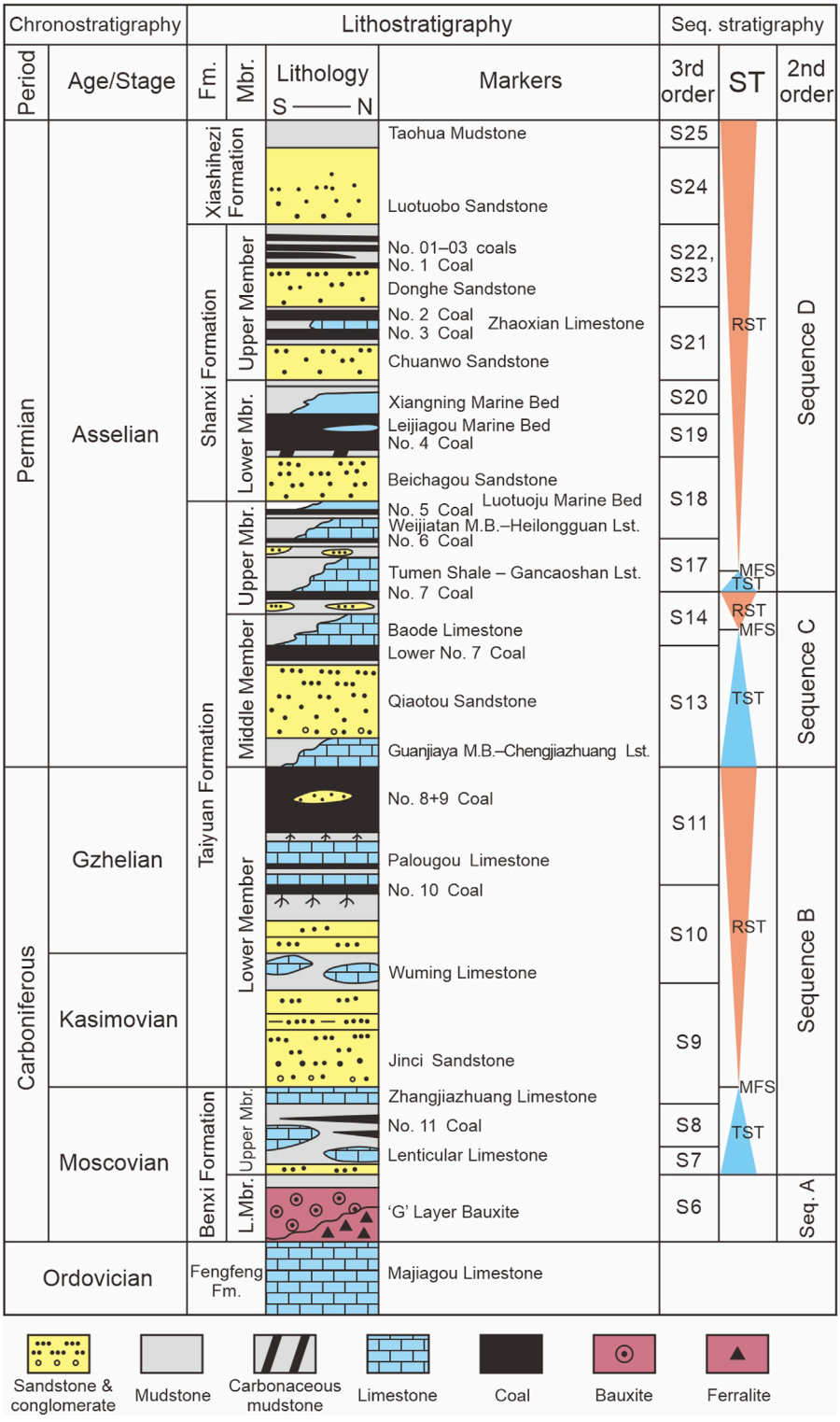

FIGURE 2
Composite stratigraphic column of the Permo-Carboniferous coal-bearing strata in the eastern Ordos Basin (chronostratigraphy from Shen et al. (2022), petrostratigraphy from Chen (1989), sequence stratigraphy from Liu, (2020)). Abbreviations: ST—systems tracts; TST—transgressive systems tract; RST—regressive systems tract; MFS—maximum flooding surface.

seams in the eastern Ordos Basin is a prerequisite for conducting in-depth theoretical research on deep/shallow CBM. The temperature of strata may be influenced by multiple factors such as burial depth, lithology, structural conditions, magmatic activity, groundwater dynamic conditions, and the thickness of Cenozoic loose layers (Tan et al., 2009; Liu et al., 2012; Zhang, 2012; Wu et al., 2013;

TABLE 1 Basic information of the coal samples in coal permeability sensitivity experiment.

Block	No.	Depth (m)	$R_{o,max}$ (%)	Initial permeability (mD)	Stress sensitivity coefficient ($^{-1}$MPa)	Maximum damage rate of permeability (%)
Cental Linxing	Lin 1	1873	1.38	0.0432	0.102	87.55
	Lin 2	1,631	1.23	0.2358	0.135	94.21
	Lin 3	1,588	1.16	0.3903	0.127	92.23
Liulin	Liu 1	546	1.29	1.8214	0.226	84.95
	Liu 2	661	1.32	1.9702	0.193	80.37
	Liu 3	982	1.25	0.1236	0.240	86.66
Yachuannan	Yan 1	1,395	2.32	0.0659	0.160	96.59
	Yan 2	1,072	2.01	0.5093	0.128	93.58
	Yan 3	1,233	2.18	0.1501	0.172	97.55
Hancheng	Han 1	709	1.9	0.4891	0.206	82.48
	Han 2	634	1.85	2.2453	0.285	91.31

Békési et al., 2020; Jiang et al., 2020). Among them, burial depth is considered the most important influencing factor. Most scholars have found through data statistics that coal seam temperature shows a linear increasing trend with increasing burial depth (Peng et al., 2017; Li et al., 2018; Békési et al., 2020), while geothermal gradient is dispersed in the shallow part of the formation and concentrated in the deep part (Yuan et al., 2009; Peng et al., 2017; Li et al., 2018). By statistically analyzing the temperature and geothermal gradient of CBM reservoirs in different areas of the eastern Ordos Basin, and plotting their relationship with the burial depth of coal seams (Figure 3), a similar pattern was found: the shallower of the coal seam, the lower the temperature of the CBM reservoir, and the wider the range of geothermal gradient changes. For example, coal seams shallower than 648 m have a maximum temperature of no more than 40°C, but their geothermal gradient changes in the range of 0.62°C–4.93°C/100 m. This indicates that the shallower the burial depth of the coal seam, the more complex the geological factors that affect the temperature of its reservoir (Lu et al., 2013); The deeper the coal seam is buried, the more stable the geological conditions are, the more significant the dominance of depth on reservoir temperature, and the stronger the linear correlation between the two. On the plane, the West Linxing Block with the deepest coal seam has the highest reservoir temperature, followed by the Central Linxing Block, with the highest reservoir temperatures reaching over 60°C. The average geothermal gradient shows a gradually increasing trend from north to south (Table 2).

4.1.2 Reservoir pressure field

The definition of CBM reservoir pressure is the pressure acting on the fluid inside the pores and fractures. It not only controls the adsorption-desorption ability of coal seams to methane and other gases but also serves as the driving force for the transportation and production of CBM (Fu et al., 2001; Yang, 2015). Li et al. (2004) found through analysis of well-testing data from 151 coal seams in China that due to a series of factors such as complex geological structure evolution, strong stratigraphic uplift and erosion, poor coal seam permeability, complex stress conditions, and variable hydrogeological conditions, CBM reservoirs are mainly under-pressure reservoirs. Regarding the relationship between CBM reservoir pressure and its gradient with burial depth, it is generally believed that there is a linear positive correlation between reservoir pressure and burial depth (Xu et al., 2010; Zhao et al., 2016; Guo et al., 2020), while the pressure gradient of CBM reservoirs has a characteristic of gradually converging from discretization as burial depth increases from shallow to deep (Qin and Shen, 2016; Chen et al., 2018a). This study collected 192 well-testing reservoir pressure data points from 13 different blocks in the eastern Ordos Basin and found similar patterns with a certain uniqueness. As shown in Figure 4, there is a good linear correlation between the CBM reservoir pressure from 427 to 2,195 m and the burial depth (R^2=0.7847), which is mainly because the pore volume compression degree and groundwater mineralization degree are higher and the water head height is lower as the depth increases (Zhong, 2003; Wu et al., 2007; Jing, 2012). However, it should be noted that within the depth range of 1,300–1,500 m, the pressure of the CBM reservoir is relatively low. As for the relationship between reservoir pressure gradient and depth, it is more complex. At depths below 1,300 m, it exhibits the characteristic of "large interval span", ranging from 0.314 to 1.25 MPa/100 m. Within the range of 1,300–1,500 m, it exhibits obvious "under-pressure" characteristics, ranging from 0.321 to 0.8

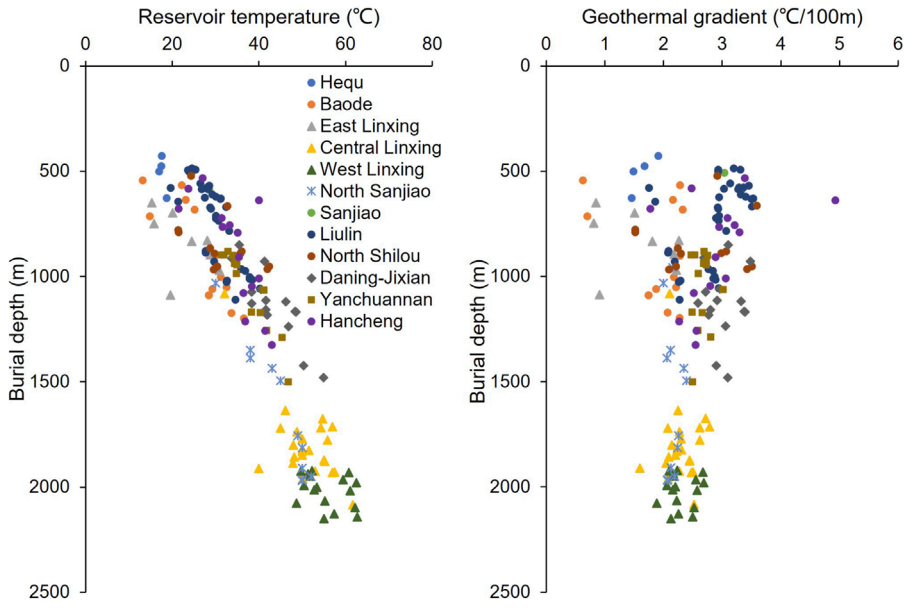

FIGURE 3
The variation law of reservoir temperature and geothermal gradient of CBM reservoirs in different areas of the eastern Ordos Basin with burial depth.

MPa/100 m. Within the range of 1,500–2,200 m, it exhibits obvious "normal to overpressure" characteristics, ranging from 0.706 to 1.169 MPa/100 m.

4.1.3 Stress field

Stress not only determines the degree of development and closure of coal seam fractures but also controls the shape and direction of fracturing fractures, thus playing an important role in controlling the permeability of CBM reservoirs (Kang et al., 2010; Meng et al., 2010; Kang et al., 2017). The gravity effect and tectonic movement are the main reasons for the formation of the stress field, with horizontal tectonic changes having the greatest impact on the distribution characteristics of the stress field (Zoback et al., 2003; Zhao et al., 2007; Ju et al., 2018). In addition, the changes in the *in-situ* stress field of different types of rocks are generally determined by the differences in the internal characteristics (composition, structure, mechanical properties, etc.) (Ward, 2016; Weniger et al., 2016; Mukherjee et al., 2021) and external environment (burial depth, temperature, pressure, etc.) of the rocks (Bell, 2006; Burra et al., 2014). Generally speaking, the *in-situ* stress increases with the increase of the Young's modulus of the rocks. In terms of horizontal stress, magmatic rocks are higher, followed by metamorphic rocks, and sedimentary rocks are generally lower (Zhu and Tao, 1994). As an organic matter aggregate with lower mechanical strength, CBM reservoirs have a lower minimum horizontal principal stress than other sedimentary rocks (Meng et al., 2011). In addition, various geological structures such as faults, folds, and collapse columns are widely developed in coal-bearing strata, and their stress heterogeneity is significant. According to the different directions of stress, stress can be divided into maximum horizontal principal stress (σ_h), minimum horizontal principal stress (σ_H), and vertical principal stress (σ_v).

Through a large amount of statistical analysis of the stress data obtained from well testing parameters and the stress data obtained from logging inversion, it was found that in addition to vertical stress, the maximum and minimum horizontal principal stresses also increase with increasing burial depth (Figure 5), which is similar to previous research results (Xu et al., 2016; Zhao et al., 2016; Chen et al., 2017; Chen et al., 2018b; Ju et al., 2021). Among them, the linear relationship between the minimum horizontal principal stress and the burial depth of the coal seam is more significant than that of the maximum horizontal principal stress. The correlation coefficient R^2 of the former is 0.8336, and the correlation coefficient R^2 of the latter is 0.6356. In the vertical direction, there is a transition surface around 1,500 m. That is, at depths smaller than 1,500 m, the relation between the maximum horizontal principal stress and the vertical stress is uncertain, while at depths more than 1,500 m, the maximum horizontal principal stress is smaller than the vertical stress. According to the magnitude of the minimum horizontal principal stress, the stress levels of CBM reservoirs at different depths can be divided into four categories, including low-stress areas ($0 < \sigma_h < 10$ MPa), medium-stress zone ($10 < \sigma_h < 18$ MPa), high-stress zone ($18 < \sigma_h < 30$ MPa), and ultra-high stress zone ($\sigma_h > 30$ MPa). Therefore, coal seams buried at depths of 500–1,000 m are mostly low to medium stress, coal seams buried at depths of 1,000–1,500 m are mostly medium to high stress, and coal seams buried below 1,500 m are mostly high to ultra-high stress. As shown in Figure 6, both the maximum and minimum horizontal principal stress gradient changes exhibit the characteristics of "strong dispersion in the shallow and strong convergence in the deep". This indicates that the shallower the coal seam is buried, the greater the influence of geological tectonic conditions on the stress field, and the more severe the differentiation of the minimum and maximum horizontal principal stress gradients. At depths of over 1000m, the minimum and maximum horizontal

TABLE 2 *In-situ* geological parameters of CBM reservoirs in different blocks in the eastern Ordos Basin.

Parameters	Hequ	Baode	East Linxing	Central Linxing	Liulin	North Shilou	Daning-Jixian	Yanchuanan	Hancheng
Depth (m)	4,27–627 508	542–1,173 791	699–1,087 839	1,069–2,161 1879	486–1,110 730	521–967 843	849–1,481 1,137	881–1,501 1,095	532–1,325 887
Reservoir Pressure (Ma)	2.7–4.6 3.3	2.6–11.8 6.2	5.1–9.3 6.9	9.43–21.22 16.5	2.2–9.9 6.0	3.8–9.9 7.3	4.6–12.1 8.3	2.8–10.6 6.3	4.1–11.9 7.3
Pressure Gradient (MPa/100 m)	0.60–0.78 0.68	0.47–0.98 0.76	0.73–0.91 0.84	0.83–1.02 0.96	0.41–1.12 0.82	0.74–1.13 0.87	0.32–0.98 0.75	0.31–0.86 0.55	0.48–1.14 0.79
σ_h (MPa)	4.0–8.8 6.9	8.2–22.1 11.7	9.8–20.8 13.4	14.32–41.39 29.08	5.8–20.9 13.75	11.2–20.8 16.5	14.7–24.1 19.7	9.0–23.2 15.3	10.0–31.9 17.6
Gradient of σ_h (MPa/100 m)	0.94–1.97 1.44	1.18–2.06 1.53	1.27–2.19 1.62	1.17–1.98 1.55	1.19–2.98 1.95	1.42–2.37 1.99	1.33–1.89 1.65	0.98–1.90 1.40	1.03–2.45 1.89
σ_H (MPa)	4.1–14.5 9.7	8.8–31.4 15.9	11.4–31.9 18.3	18.72–58.16 36.82	3.63–32.8 20.46	13.0–32.3 24.5	22.1–40.5 30.0	9.5–37.2 21.6	9.3–53.3 26.2
Gradient of σ_H (MPa/100 m)	0.97–3.24 2.04	1.24–3.02 2.11	1.41–3.35 2.23	1.39–2.81 1.96	0.74–4.78 2.90	1.52–3.68 2.95	1.90–2.92 2.49	1.07–3.00 1.97	1.23–4.99 2.96
Reservoir temperature (°C)	17.0–18.7 17.7	13.2–36.5 24.3	15.3–30.9 22.9	32.1–62.5 52.2	19.6–40.2 30.0	21.4–42.35 31.2	33.7–54.9 43.5	31.5–46.8 37.4	21.5–43.0 34.3
Gradient of temperature (°C/100 m)	1.46–1.91 1.64	0.62–2.33 1.88	0.81–2.26 1.57	1.59–2.79 2.31	1.75–3.53 2.88	1.52–3.51 2.62	2.58–3.48 3.01	2.48–3.02 2.66	1.78–4.93 2.92

10.3389/feart.2024.1416308

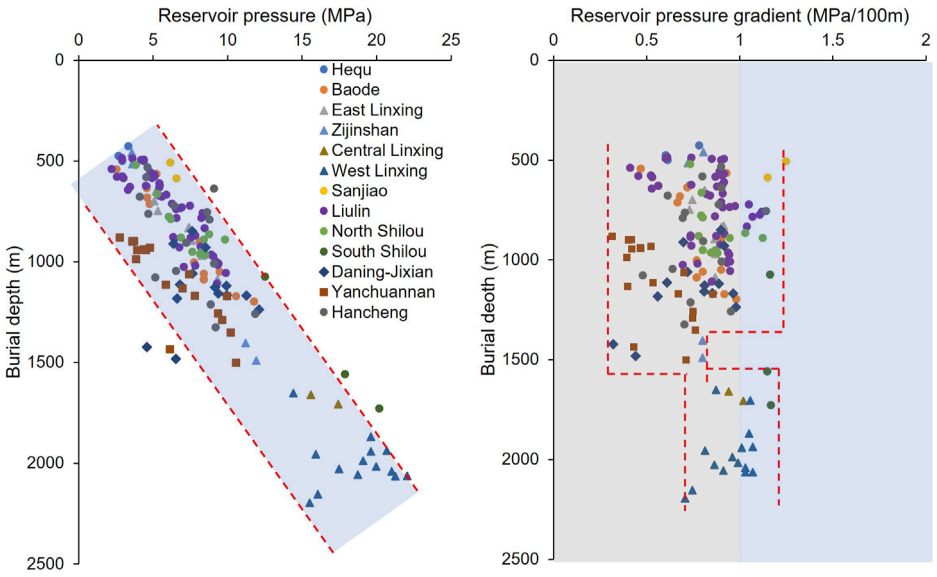

FIGURE 4
The variation law of CBM reservoir pressure and reservoir pressure gradient with burial depth in the eastern Ordos Basin.

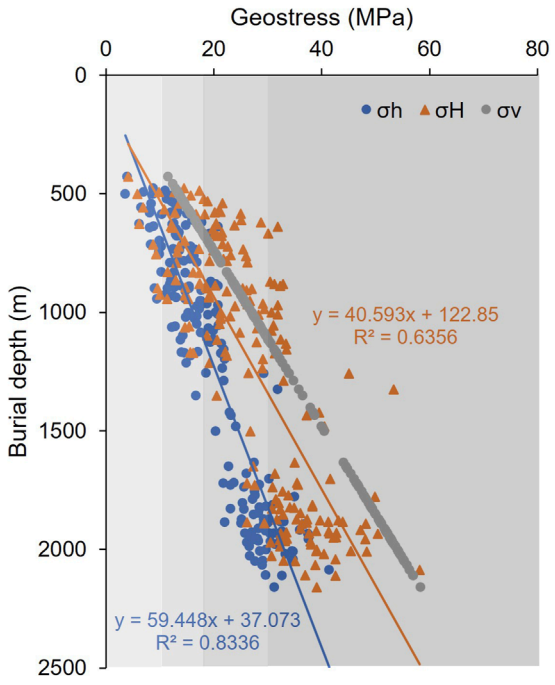

FIGURE 5
The variation law of coal seam stress with burial depth in the eastern Ordos Basin.

principal stress gradients decrease to below 2 MPa/100m and 3 MPa/100m, respectively.

Regarding the variation of lateral pressure coefficient (the ratio of average horizontal principal stress to vertical stress), Brown and Hock (1980) summarized the relationship between lateral pressure coefficient and coal seam burial depth through a large amount of stress data from different regions around the world. That is, the lateral pressure coefficient of shallow coal seams is higher, and the variation range is larger, and as the burial depth increases, both the lateral pressure coefficient and the variation range continuously decrease. The above characteristics indicate that the shallow CBM reservoir is mainly dominated by horizontal stress, while the direction of the main stress in the deep CBM reservoir gradually changes to vertical. Zhao et al. (2007) drew inspiration from Hoek and Brown's stress research method and fitted a regression curve between China's lateral pressure coefficient and burial depth. They compared it with Hoek and Brown's global stress statistical regression curve, showing that China's stress has a similar vertical evolution law to the world's, and pointed out that the critical depth is around 1,000 m. This study found that the lateral pressure coefficient of CBM reservoirs in the eastern Ordos Basin shows a characteristic of "dispersion at shallow and convergence at deep" in the vertical direction and is overall above the Chinese average line and the Hoek and Brown's average line, that is, the lateral pressure coefficient of coal seams is smaller under the same burial depth conditions, which is largely related to the lower mechanical strength of coal rock compared to other rock layers (Figure 7). In addition, there is a transition interface between the lateral pressure coefficient and the depth of the coal seam, with a wide distribution range of lateral pressure coefficients ranging from 0.31 to 1.53 below 1,000 m; At depths of 1,000 m or more, the lateral pressure coefficient is generally less than 1.

The relative magnitude of σ_v, σ_h, and σ_H can reflect different *in-situ* stress mechanisms. Where $\sigma_v > \sigma_H > \sigma_h$ represents the normal fault stress mechanism, that is, overlying gravity load dominates; $\sigma_H > \sigma_v > \sigma_h$ represents the mechanism of reverse fault stress and $\sigma_H > \sigma_h > \sigma_v$ represents the mechanism of strike-slip fault stress, representing two forms of structural compression in different directions. Figure 8 shows the stress field types of different blocks in the eastern Ordos Basin. The Hequ, Baode, East Linxing, and

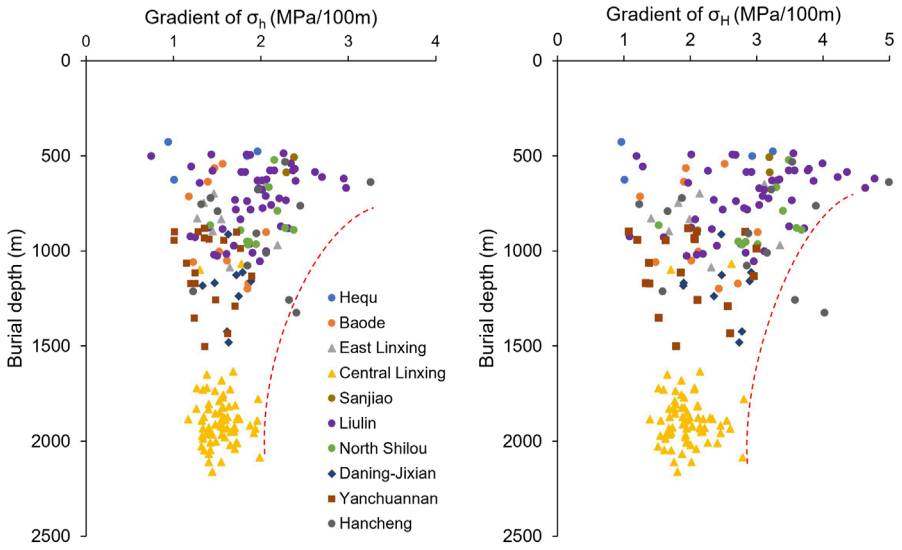

FIGURE 6
Variation law of minimum/maximum horizontal principal stress gradient with burial depth in the eastern Ordos Basin.

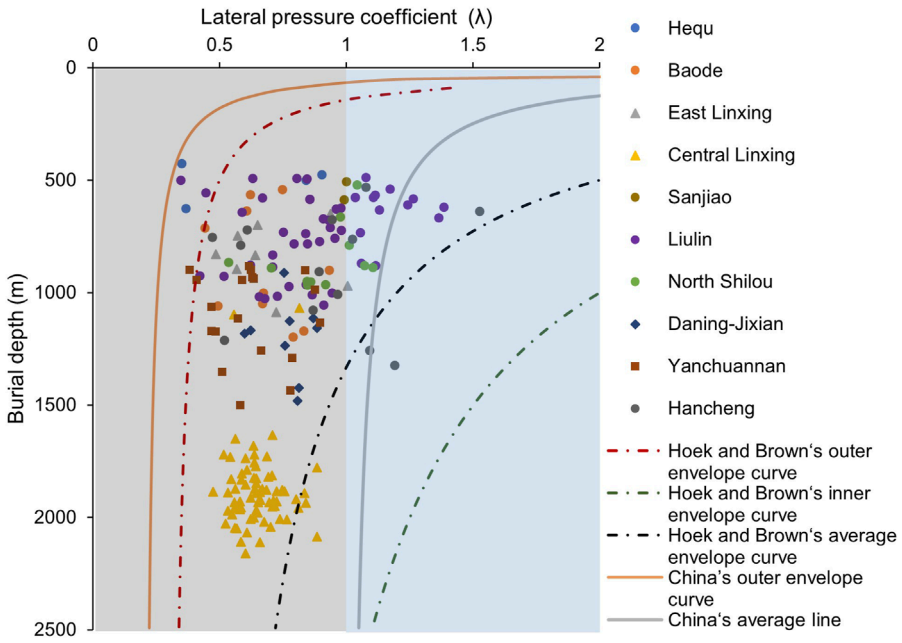

FIGURE 7
Vertical evolution of lateral pressure coefficient of CBM reservoir in the eastern Ordos Basin.

Central Linxing blocks show $\sigma_v > \sigma_H > \sigma_h$ type stress field as a whole. The reason is that Hequ, Baode, and Linxing Dong were affected by the NW-SE stretching and developed a series of northeastward normal faults (Chen et al., 2014) during the Himalayan period, while the coal seam in central Linxing Block was buried too deep and the structure was relatively stable. In Sanjiao, Liulin, and North Shilou blocks in central China, 62.90% of the CBM reservoirs exhibit $\sigma_H > \sigma_v > \sigma_h$ type stress field, 33.87% exhibit $\sigma_v > \sigma_H > \sigma_h$ type, and 3.23% exhibit $\sigma_H > \sigma_h > \sigma_v$ type, indicating that the stress mechanism of inverse fault is dominant and that of normal fault is supplemented. To the Daning-Jixian, and Yanchuannan blocks, the stress state transitioned to the normal fault stress mechanism ($\sigma_v > \sigma_H > \sigma_h$), with local reverse fault stress mechanism ($\sigma_H > \sigma_v > \sigma_h$). To the southernmost Hancheng Block, the stress state of CBM reservoir is again transformed into the reverse fault type compressive stress field, that is, $\sigma_H > \sigma_v > \sigma_h$, which is

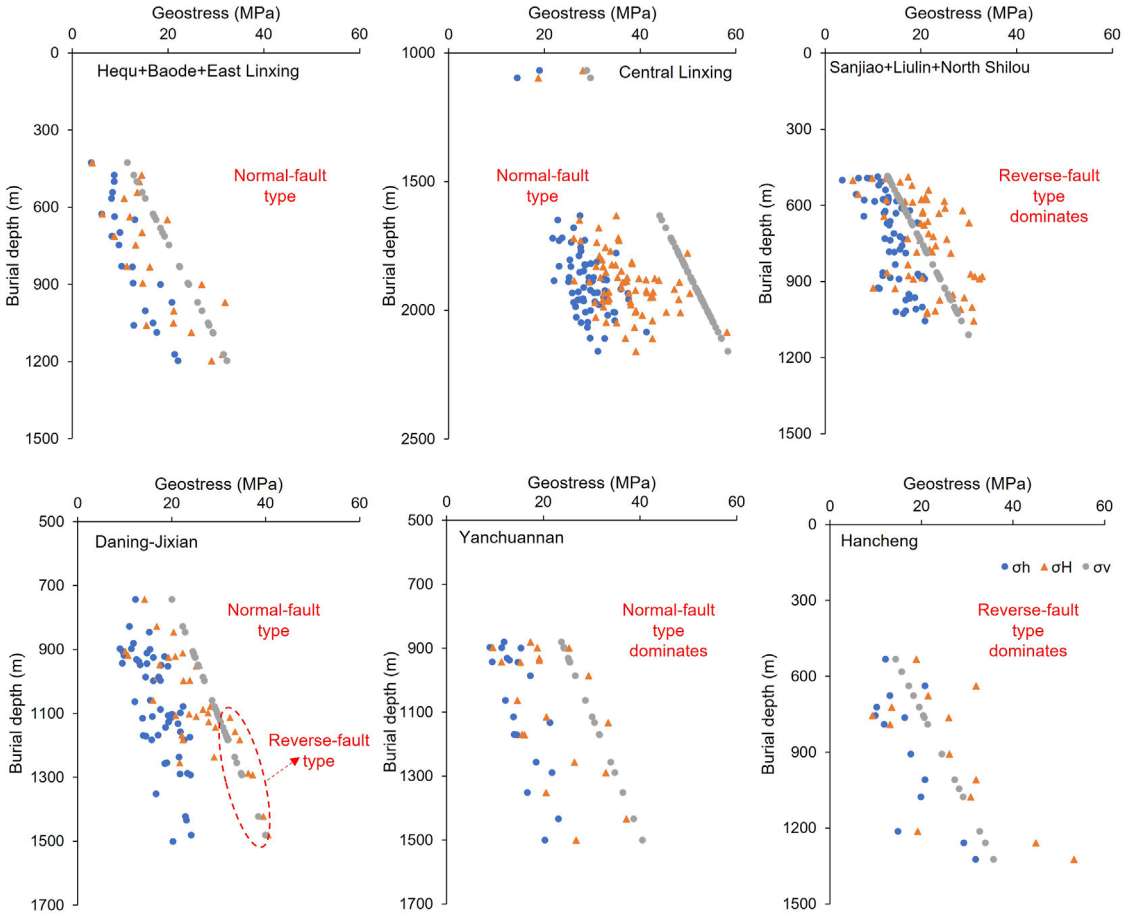

FIGURE 8
Stress field types of different blocks in the eastern Ordos Basin.

consistent with the structural density. On the whole, the stress fields of three deep blocks, including central Linxing, Daning-Jixian and Yanchuannan, are normal fault-type stress mechanisms dominated by vertical stress. Among them, the Yanchuannan has the most significant normal fault-type stress mechanism, and it has the lowest average maximum/minimum horizontal principal stress gradient and reservoir pressure gradient in the eastern Ordos basin (Table 2).

4.2 *In-situ* permeability

The permeability characteristics of CBM reservoirs directly determine the effectiveness of CBM development and are important parameters for evaluating the potential of CBM extraction and selecting favorable areas. At present, there are various methods for measuring permeability, including core laboratory testing, well-testing, reservoir simulation, and well logging inversion. Among them, injection/pressure drop well-testing permeability is the most widely used and can better reflect the characteristics of *in-situ* permeability. This study statistically analyzed 140 well-testing permeability data from 9 different blocks (Figure 9). Among them, the permeability of Hequ, Baode, and East Linxing in the northern part is the highest, mainly distributed in 0.1–10 mD. The permeability of Sanjiao, Liulin, and North Shilou in the middle is lower than that in the north, mainly distributed in 0.01–1 mD, and there are locally high permeability areas greater than 1 mD. The permeability variation range of the 5# coal seam in the Daning-Jixian Block is 0.004–6.74 mD, and the permeability of the 8# coal seam is between 0.008 and 4.36 mD, with a large variation amplitude and a decreasing trend with the increase of coal seam burial depth. The permeability distribution of the 2# coal reservoir in the Yanchuannan Block is between 0.013 and 0.99 mD, with an average of 0.224 mD. The southernmost Hancheng Block has a permeability distribution of 0.003–4.52 mD, with an average of 0.41 mD. The permeability of CBM reservoir generally decreases with the increase of burial depth, but the deep stress release zone can also have high permeability, showing a large regional difference (Mukherjee et al., 2020; 2021). In the Daning-Jixian Block, the Taoyuan anticline axis and vicinity of faults are high-permeability zones (Li et al., 2019). In the Yanchuannan Block, high-permeability zones are distributed in areas with higher structural elevation and relatively well-developed small fault zones (Chen et al., 2019; Zhang et al., 2020). In the central Linxing Block, the intrusion of Zijinshan rock mass has a strong reforming effect on the permeability of coal reservoir (Pu et al., 2022).

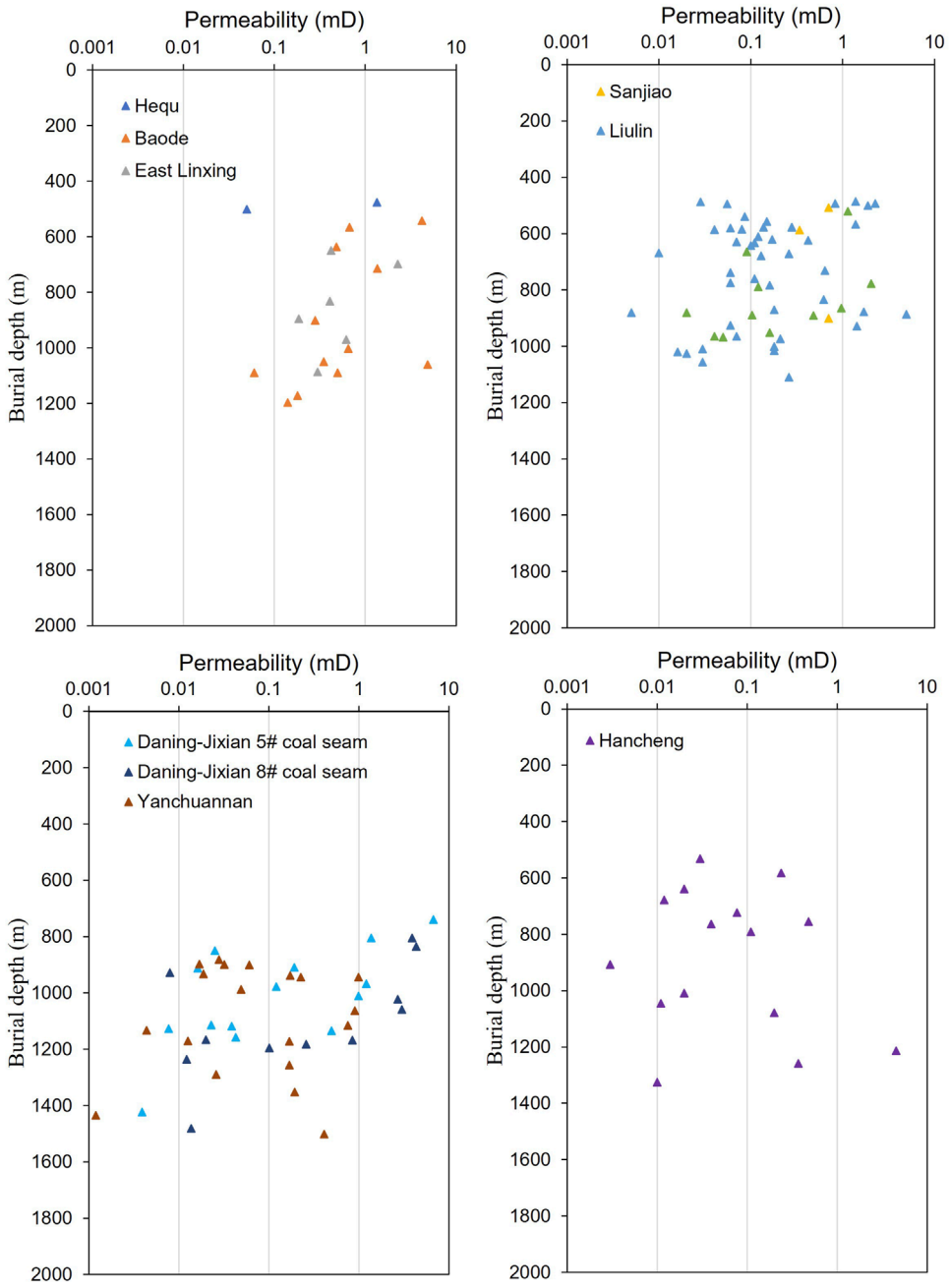

FIGURE 9
Distribution of well test permeability with burial depth in different blocks in the eastern Ordos Basin.

4.3 Permeability sensitivity analysis

4.3.1 Stress sensitivity analysis

As shown in Figure 10, the permeability of coal decreases in a negative exponential form with the increase of effective stress. The fitting curve formula can be uniformly expressed as follows:

$$K = \alpha e^{-bP} \quad (1)$$

In Eq. 1, K is the gas permeability of coal under given effective stress conditions, mD; P is the equivalent effective stress, MPa; α is the gas permeability of coal at an effective stress of 0 MPa, i.e., the initial permeability of coal; b is the permeability modulus, also known as the stress sensitivity coefficient of permeability, MPa^{-1}. The larger the value of b, the more sensitive the coal permeability as effective stress changes, that is, within the same stress variation range, the greater the decrease in gas permeability (Wu et al., 2017).

The fitting results of 11 samples all have a high correlation, with correlation coefficients between 0.9735 and 0.9998. The fitting results show that the initial permeability of the samples is between 0.0432 and 2.2453 mD. Overall, the original permeability of coal in the central Linxing and Yanchuannan blocks is significantly lower than that in the Liulin and Hancheng, which is consistent with

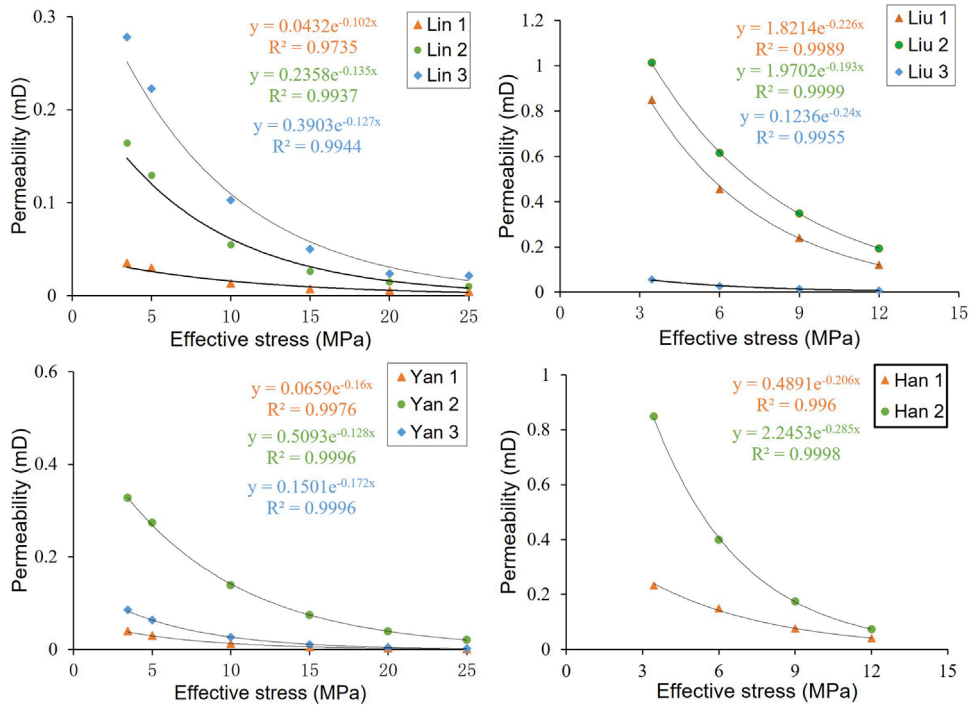

FIGURE 10
The variation law of coal permeability with effective stress increase.

the low permeability characteristics of deep CBM reservoirs. At the same time, the fitting curve shows that under experimental conditions, the stress sensitivity coefficient of coal rock samples is between 0.102 and 0.285, and there is a significant difference in stress sensitivity between blocks. The relative sizes are Central Linxing < Yanchuannan < Liulin < Hancheng, with corresponding mean values of 0.121, 0.153, 0.220, and 0.246 $^{-1}$MPa, respectively (Figure 10; Table 1). This is characterized by the lower the initial permeability value, the smaller the stress sensitivity coefficient. On the contrary, the greater the initial permeability, the larger the stress sensitivity coefficient, and the faster the stress damage.

It can also be seen from Figure 10 that the 11 coal samples tested overall reflect the following rules: when the effective stress is below 10 MPa, the CBM reservoir has strong stress sensitivity, and the permeability decreases exponentially as the effective stress increases; After the effective stress is greater than 10 MPa, the permeability of the CBM reservoir slowly decreases with the increase of effective stress, and the stress sensitivity weakens. To further quantitatively characterize the change of coal permeability with effective stress, the concepts of permeability stage damage rate (D_{ki}) and permeability maximum damage rate (D_{km}) are introduced.

D_{ki} refers to the proportion of permeability reduction before and after pressurization, and its calculation formula can be expressed as:

$$D_{ki} = \frac{K_i - K_{i+1}}{K_i} \times 100\% \quad (2)$$

Where K_i is the permeability of coal at the i th pressure point, mD; K_{i+1} is the permeability of coal at the $i+1$ th pressure point.

The maximum damage rate of permeability (D_{km}) refers to the damage rate after the confining stress increases to the highest stress point, which can be expressed as:

$$D_{km} = \frac{K_1 - K_{min}}{K_1} \times 100\% \quad (3)$$

Where K_1 is the coal permeability at the first pressure point, mD; K_{min} is the minimum permeability of coal achieved after applying the maximum effective stress.

Figure 11 shows the trend of permeability damage rate of 11 coal rock samples with increasing effective stress. It can be seen that as the effective stress increases, the trend of the curve slows down, that is, the permeability stage damage rate (Eq. 2) decreases with the increase of effective stress, and the cumulative damage rate continuously increases until it reaches the maximum damage rate. The maximum permeability damage rate (Eq. 3) of 11 samples ranges from 80.37% to 97.55%. Among them, the maximum permeability damage rate of coal in Liulin and Hancheng areas is mostly less than 90%, with an average of 83.99% and 86.90%, respectively. In contrast, the maximum permeability damage rate of coal samples in central Linxing and Yanchuannan during the entire pressurization process is basically above 90%, with an average of 91.33% and 95.91%, respectively.

4.3.2 Temperature sensitivity analysis

With the increasing depth of CBM extraction, the influence of temperature on the permeability of CBM reservoirs is also receiving more and more attention. As shown in Figure 12, when the same coal sample is subjected to the same effective stress, the higher the temperature, the lower the permeability of coal, and the overall negative effect of temperature is exhibited. This negative effect is mainly concentrated under conditions where the effective stress is less than 10 MPa, and gradually weakens as the effective stress increases.

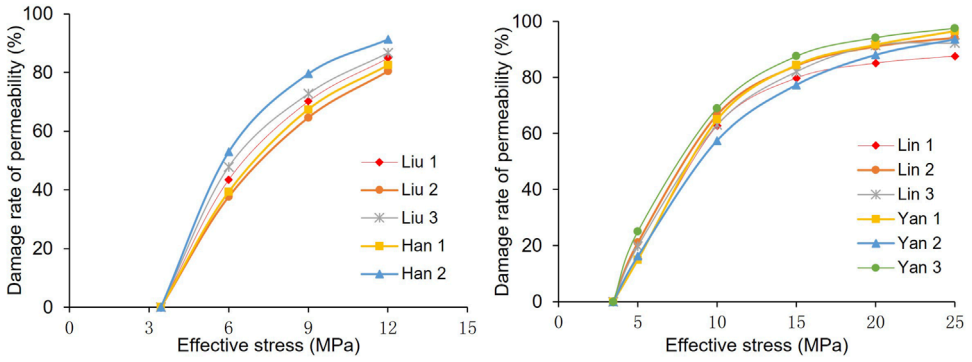

FIGURE 11
Variation law of permeability damage rate of coal rock with the increase of effective stress.

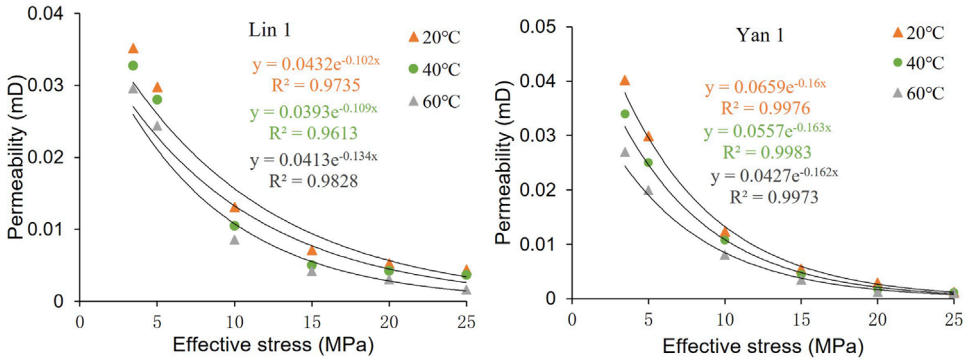

FIGURE 12
Superimposed effect of stress and temperature sensitivity on coal permeability.

This is because the coal skeleton undergoes thermal expansion with increasing temperature, causing a reduction in methane migration channels and a decrease in coal permeability (Yang et al., 2005b). However, when the effective stress is high, the pore and fracture space in the coal has been greatly compressed, and the expansion space of the coal matrix is extremely limited, so the negative effect of temperature is no longer significant. In addition, it can be observed that the higher the temperature, the greater the stress sensitivity coefficient of coal rock permeability, and the faster the permeability damage (Figure 12). Overall, both high temperature and high-stress conditions can damage the permeability of coal, but the impact of temperature on the permeability of CBM reservoirs is much smaller than stress, especially under high-stress conditions.

4.3.3 Depth effect of coal permeability sensitivity

The depth effect of reservoir permeability sensitivity is complex. The influence of depth on coal permeability is reflected in many aspects, such as stress conditions, temperature, pore pressure, initial permeability difference, and material composition, etc., but the basic reason is the compression difference of coal pores and fractures under different depths and stress conditions (Burra et al., 2014; Zhang et al., 2019). Therefore, the geological conditions and *in-situ* conditions of different depths and regions are various, and the evolution of permeability related parameters with depth is also different, but there are basic rules to follow in the same region. As shown in Figure 13, the initial permeability and stress sensitivity coefficient of coal in the four blocks are strongly negatively correlated with the depth of coal seam, and positively correlated with the maximum damage rate of permeability. That is, the deeper the coal seam is, the lower the permeability and stress sensitivity coefficient are, and the slower the permeability damage will be in the process of CBM drainage and production. However, when the reservoir pressure drops to the depletion pressure, the maximum damage rate of permeability increases. During the development process of shallow CBM, the permeability can be maintained at a relatively high level, which is beneficial for mining and is in good agreement with the actual mining situation. As far as deep CBM is concerned, its initial permeability is very low and is getting worse during the development process. Taking several deep CBM Wells in Central Linxing Block as an example, although most of them have obtained industrial gas flow in the gas testing stage and their resource conditions have been proved to be excellent, most of them in the drainage stage show the characteristics of short initial gas discovery time, low water production and short stable production time (Chen et al. 2024a). Therefore, for deep CBM, a completely different approach should be adopted from shallow CBM.

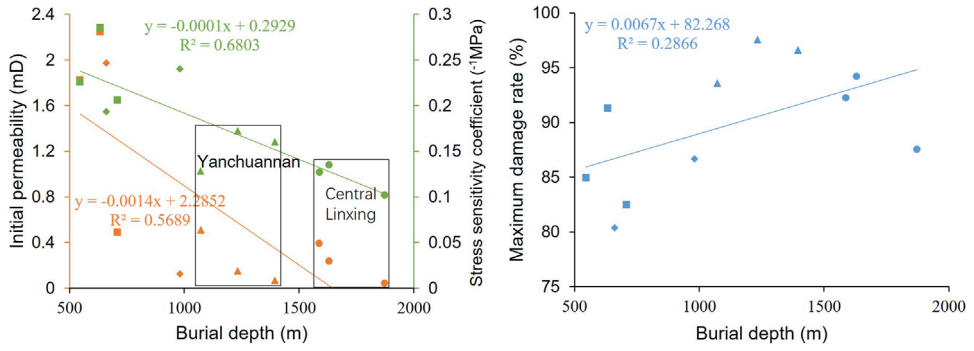

FIGURE 13
Depth effect of stress sensitivity.

4.4 Implications for deep CBM development

The exploration paradigm for deep CBM has shifted from targeting resource sweet spots to high-production sweet spots (Xu et al., 2022). High-production zones must not only possess a certain level of resource abundance but also exhibit relatively high permeability and low stress, enabling extensive reservoir reconstruction measures (Song et al., 2016). Drawing from the practical development outcomes of deep CBM blocks, two primary types of favorable zones can be discerned. One type is the structural high section with a broad and gentle configuration (positive micro-amplitude structure zone), denoting the coal reservoir that underwent deep burial initially, followed by a certain degree of structural uplift, leading to shallower burial depth of the local coal seam and development of secondary cleats. This results in increased permeability; however, without significant structural damage to the roof and floor, the original gas reservoir remains relatively well-preserved. The release of *in-situ* stress forms a relatively low-stress area, with the two wings of the high section serving as conduits for gas migration to the top. This facilitates the formation of CBM-enriched and high-yield regions with high gas content, saturation, and permeability. For instance, wells W7-5 and W6-10X1 in the Hukou slope of the Daning-Jixian Block exhibit stable gas production ranging from 4,000 to 5,000 m^3/d (Yan et al., 2021). The Yan 16 well group in the southern segment of the Wanbaoshan structural belt in the Yanchuannan Block has maintained stable production exceeding 2,000 m^3/d for 8 years, with a peak daily production of 8,000 m^3/d (Chen et al., 2024b). The other type is the upper slope of the enrichment area, formed at the top of the slope belt due to the combined effects of compressive stress and uneven crustal uplift. Taking the Daning-Jixian Block as an example, the western part of the Taoyuan anticline represents a west-dipping monoclinic structure. The upper slope zone in this region showcases the best superimposition effect of gas content, permeability, and *in-situ* stress characteristics. For example, Daning-Jixian's TU1 and TL1 wells achieved average production of 1,266.82 m^3/d and 2,827.21 m^3/d respectively, and cumulative gas production of 3,409,006 m^3 and 5,962,587 m^3 (Zhang et al., 2022).

Due to the low permeability of deep CBM reservoirs that characterized by primary and fragmented structures, vertical stress predominating, a lateral pressure coefficient less than 1, making the formation of horizontal and long fractures challenging during the vertical well fracturing process. The CBM development practices in the Yanchuannan Block, Daning-Jixian Block, and Qinshui Basin have demonstrated that the vertical well + horizontal well combination mode not only reduces well spacing but also interconnects a large number of fracture systems, facilitating regional pressure reduction and enhancing the utilization of CBM reserves (Zhu et al., 2019; Jiang and Yang, 2021; Zhang et al., 2022). Deep CBM reservoirs exhibit large horizontal principal stress differences, and artificially expanded fractures often intersect natural fractures directly, posing challenges in forming a three-dimensional fracture network (Dunlop et al., 2017). This issue has been addressed in the Yanchuannan and Daning-Jixian blocks through the implementation of high liquid volume (1,016–6,874 m^3) and large-scale fracturing measures (Yan et al., 2021; Chen et al., 2024b). The effective fracturing approach of "creating long fractures and remote support" in deep high-stress environments has led to a breakthrough in the productivity of deep CBM wells (Yan et al., 2021).

In contrast to shallow CBM reservoirs which are predominantly undersaturated, deep CBM reservoirs, under the coupled control of high temperature and pressure conditions, contain a significant amount of saturated to supersaturated gas reservoirs (Kang et al., 2019). Given the permeability sensitivity of deep coal reservoir, the conventional "continuous, stable, long-term, slow" drainage method suitable for shallow CBM is no longer viable. Production practices in the Yanchuannan Block have shown that rapid depressurization, coupled with effective fracturing and support, is more conducive to achieving efficient and stable high yield in deep CBM wells (Zhao et al., 2021). This is primarily attributed to the fact that effective fracturing and support can to some extent mitigate reservoir stress sensitivity effects; rapid depressurization can prompt rapid desorption and accumulation of CBM in the near-well region during the rapid or sensitive desorption stage, while enhancing coal-rock matrix shrinkage effects to drive subsequent gas production; rapid depressurization can also increase reservoir pressure differentials near and far from the wellbore, enhancing gas mass transfer efficiency in low-permeability CBM reservoirs (Su et al., 2019; Zhao et al., 2021). Building on the successful experience of the Yanchuannan Block, the application of rapid

depressurization in deeper-buried coal reservoirs with higher gas saturation in the Daning-Jixian and Central Linxing blocks warrants further theoretical exploration and practical validation.

5 Conclusion

This study integrates extensive *in-situ* geological data from the eastern Ordos Basin and conducts coal permeability sensitivity experiments to dissect the fundamental reasons for significant production capacity differences between deep and shallow blocks and promote mutual learning from successful development experiences. The main conclusions drawn are as follows:

(1) Shallower coal seams usually have lower temperatures and a wider variation range of geothermal gradients. Reservoir temperature is more heavily influenced by depth in deeper coal seams.

(2) CBM reservoir pressure increases linearly with burial depth within the range of 427–2,195 m, with localized pressure low anomalies observed at depths of 1,300–1,500 m. The pressure gradient spans from 0.314 to 1.25 MPa/100 m at depths below 1,300 m, while 1,300–1,500 m is the "under-pressure zone" and 1,500–2,200 m is the "normal to overpressure zone.

(3) The vertical conversion interface of stress is located at 1,500 m, below which the vertical stress is dominant. The horizontal stress gradient and lateral stress coefficient both exhibit the characteristic of "strong dispersion in shallow areas and strong convergence in deep areas" with a critical depth of 1,000 m. The stress field of CBM reservoirs is the result of the coupling effect of tectonic condition and burial depth.

(4) *In-situ* permeability of CBM reservoirs decreases with increasing burial depth, primarily influenced by tectonic stress fields. Stress release zones in deep CBM reservoirs often exhibit high permeability, emphasizing the importance of reservoir optimization and reconstruction for efficient CBM development.

(5) Deep CBM high-yield areas are typically found in structurally elevated regions with wide, gentle morphology and in the upper slope in gas-rich zones. It is advised to utilize a combination of vertical + horizontal wells and employ a fracturing technique featuring "large-scale, high-volume, multi rounds, continuous proppant injection". Additionally, implementing a "rapid depressurization" drainage system is recommended to optimize production and efficiency.

Data availability statement

The original contributions presented in the study are included in the article/Supplementary Material, further inquiries can be directed to the corresponding author.

Author contributions

YZ: Conceptualization, Data curation, Formal Analysis, Investigation, Methodology, Software, Validation, Visualization, Writing–original draft, Writing–review and editing. JL: Formal Analysis, Software, Validation, Writing–review and editing.

Funding

The author(s) declare that financial support was received for the research, authorship, and/or publication of this article. This research was funded by National Natural Science Foundation of China (grant number 42230812) and the Postdoctoral Fellowship Program of CPSF (grant number GZC20233110).

Acknowledgments

We acknowledge the editors and reviewers for critical review and constructive comments.

Conflict of interest

Authors YZ and JL were employed by PetroChina.

Publisher's note

All claims expressed in this article are solely those of the authors and do not necessarily represent those of their affiliated organizations, or those of the publisher, the editors and the reviewers. Any product that may be evaluated in this article, or claim that may be made by its manufacturer, is not guaranteed or endorsed by the publisher.

References

Békési, E., Struijk, M., Bonté, D., Veldkamp, H., Limberger, J., Fokker, P. A., et al. (2020). An updated geothermal model of the Dutch subsurface based on inversion of temperature data. *Geothermics* 88, 101880. doi:10.1016/j.geothermics.2020.101880

Bell, J. S. (2006). *In-situ* stress and coal bed methane potential in Western Canada. *Bull. Can. Petroleum Geol.* 54 (3), 197–220. doi:10.2113/gscpgbull.54.3.197

Brown, E. T., and Hock, E. B. (1980). *Underground excavations in rock*. London: The institute of minng and metallurgy.

Burra, A., Esterle, J. S., and Golding, S. D. (2014). Horizontal stress anisotropy and effective stress as regulator of coal seam gas zonation in the Sydney Basin, Australia. *Int. J. coal Geol.* 132, 103–116. doi:10.1016/j.coal.2014.08.008

Chapman, D. S., Keho, T., Bauer, M. S., and Picard, M. D. (1984). Heat flow in the Uinta Basin determined from bottom hole temperature (BHT) data. *Geophysics* 49 (4), 453–466. doi:10.1190/1.1441680

Chatterjee, R., Paul, S., and Pal, P. K. (2019). Relation between coalbed permeability and *in-situ* stress magnitude for coalbed methane exploration in Jharia and Raniganj coalfields, India. *Lead. Edge* 38 (10), 800–807. doi:10.1190/tle38100800.1

Chen, B., Li, S., Tang, D., Pu, Y., and Zhong, G. (2024a). Evaluation of recoverable potential of deep coalbed methane in the linxing block, eastern margin of the Ordos Basin. *Sci. Rep.* 14 (1), 9192. doi:10.1038/s41598-024-59128-x

Chen, H., Jiang, B., Qu, Z., Wang, J., and Wang, L. (2014). Diversity structural characteristics and control action on coal bed gas content in Linfen and Baode area. *J. China Coal Soc.* 39 (3), 510–517. doi:10.13225/j.cnki.jccs.2013.1574

Chen, S., Tang, D., Tao, S., Xu, H., Li, S., and Zhao, J. (2018a). Statistic analysis on macro distribution law of geostress field in coalbed methane reservoir. *Coal Sci. Technol.* 46 (6), 57–63. doi:10.13199/j.cnki.cst.2018.06.010

Chen, S., Tang, D., Tao, S., Xu, H., Li, S., Zhao, J., et al. (2017). *In-situ* stress measurements and stress distribution characteristics of coal reservoirs in major coalfields in China: implication for coalbed methane (CBM) development. *Int. J. Coal Geol.* 182, 66–84. doi:10.1016/j.coal.2017.09.009

Chen, S., Tang, D., Tao, S., Xu, H., Zhao, J., Fu, H., et al. (2018b). *In-situ* stress, stress-dependent permeability, pore pressure and gas-bearing system in multiple coal seams in the Panguan area, western Guizhou, China. *J. Nat. Gas Sci. Eng.* 49, 110–122. doi:10.1016/j.jngse.2017.10.009

Chen, S., Tao, S., and Tang, D. (2024b). *In situ* coal permeability and favorable development methods for coalbed methane (CBM) extraction in China: from real data. *Int. J. Coal Geol.* 284, 104472. doi:10.1016/j.coal.2024.104472

Chen, Z. (1989). *Sedimentary environment and coal accumulation law of late Paleozoic coal-bearing rock series in the eastern margin of Ordos Basin*. Wuhan: China University of Geosciences Press.

Chen, Z., Guo, T., Li, X., Xiao, C., and Jin, X. (2019). Enrichment law and development technology of deep coalbed methane in South Yanchuan Coalbed Methane Field. *Coal Sci. Technol.* 47 (9), 112–118. doi:10.13199/j.cnki.cst.2019.09.011

Cheng, R., Chen, H., Xian, X., and Wang, G. (1998). Experimental study on the influence of temperature on permeability coefficient of coal sample. *Coal Eng.* (1), 13–16.

Dabbous, M., Reznik, A., Taber, J., and Fulton, P. (1974). The permeability of coal to gas and water. *Soc. Petroleum Eng. J.* 14 (06), 563–572. doi:10.2118/4711-a

Dunlop, E., Warner, D., Warner, P. E., and Coleshill, L. (2017). Ultra-deep Permian coal gas reservoirs of the Cooper Basin: insights from new studies. *APPEA J.* 57 (1), 218–262. doi:10.1071/aj16015

Fu, H., Yan, D., Yang, S., Wang, X., Zhang, Z., and Sun, M. (2020). Characteristics of *in situ* stress and its influence on coalbed methane development: a case study in the eastern part of the southern Junggar Basin, NW China. *Energy Sci. Eng.* 8 (2), 515–529. doi:10.1002/ese3.533

Fu, X., Qin, Y., Xue, X., Li, G., and Wang, W. (2001). Research on fractals of pore and fracture-structure of coal reservoirs. *J. China Univ. Min. Technol.* 30 (3), 225–228. doi:10.3321/j.issn:1000-1964.2001.03.003

Gan, J., Wu, D., Zhang, Y., Liu, S., Guo, M., Li, X., et al. (2019). Distribution pattern of present-day formation temperature in the qiongdongnan basin: implications for hydrocarbon generation and preservation. *Geol. J. China Univ.* 25 (6), 952–960. doi:10.16108/j.issn1006-7493.2019053

Gao, X. (2019). *Study on porosity and permeability evolution mechanism and fracturing reconstruction feasibility of deep coal reser-voirs in linxing area*. Beijing: China University of Mining and Technology.

Guo, M., Song, P., Zhang, B., Chen, M., and Wu, W. (2020). Origin and evolution of paleo- overpressure in the Upper Paleozoic in Linxing area, the eastern margin of Ordos Basin. *J. Xi'an Shiyou Univ. Nat. Sci. Ed.* 35 (4), 19–25. doi:10.3969/j.issn.1673-064X.2020.04.003

Harpalani, S., and Chen, G. (1992). "Effect of gas production on porosity and permeability of coal," in Proceedings of the Symposium of Coalbed Methane R and D in Australia, Townsville, Australia, 19 - 21 November 1992, 67–73.

Jiang, X., Wu, C., Zhang, E., and Zhang, S. (2020). Geotemperature-geopressure system and its distribution characteristics of Yuwang block in Laochang mining area. *J. Henan Polytech. Univ. Nat. Sci.* 39 (2), 32–37. doi:10.16186/j.cnki.1673-9787.2020.2.5

Jiang, Y., and Yang, S. (2021). New technology of dewatering gas recovery for CBM wells in southern Yanchuan Block, eastern margin of Ordos Basin. *Petroleum Reserv. Eval. Dev.* 11 (3), 384–389. doi:10.13809/j.cnki.cn32-1825/te.2021.03.013

Jing, X. (2012). Study on pressure distribution law and control factors of coal bed methane reservoir in south part of Qinshui Basin. *Coal Sci. Technol.* 40 (2), 116–120. doi:10.13199/j.cst.2012.02.121.jingxp.004

Ju, W., Yang, Z., Qin, Y., Yi, T., and Zhang, Z. (2018). Characteristics of *in-situ* stress state and prediction of the permeability in the Upper Permian coalbed methane reservoir, western Guizhou region, SW China. *J. Petroleum Sci. Eng.* 165, 199–211. doi:10.1016/j.petrol.2018.02.037

Ju, W., Yang, Z., Shen, Y., Yang, H., Wang, G., Zhang, X., et al. (2021). Mechanism of pore pressure variation in multiple coal reservoirs, western Guizhou region, South China. *Front. Earth Sci.* 15, 770–789. doi:10.1007/s11707-021-0888-7

Kang, H., Jiang, T., Zhang, X., and Yan, L. (2009). Research on *in-situ* stress field in Jincheng mining area and its application. *Chin. J. Rock Mech. Eng.* 28 (1), 1–8. doi:10.3321/j.issn:1000-6915.2009.01.001

Kang, H., Yi, B., Gao, F., and Lv, H. (2019). Database and characteristics of underground in–situ stress distribution in Chinese coal mines. *J. China Coal Soc.* 44 (1), 23–33. doi:10.13225/j.cnki.jccs.2018.5032

Kang, H. P., Zhang, X., Si, L. P., Wu, Y., and Gao, F. (2010). *In-situ* stress measurements and stress distribution characteristics in underground coal mines in China. *Eng. Geol.* 116 (3-4), 333–345. doi:10.1016/j.enggeo.2010.09.015

Kang, Y., Sun, L., Zhang, B., Gu, J., Ye, J., Jiang, S., et al. (2017). The controlling factors of coalbed reservoir permeability and CBM development strategy in China. *Geol. Rev.* 63 (5), 1401–1418. doi:10.16509/j.georeview.2017.05.019

Karacan, C., and Okandan, E. (2001). Adsorption and gas transport in coal microstructure: investigation and evaluation by quantitative X-ray CT imaging. *Fuel* 80 (4), 509–520. doi:10.1016/s0016-2361(00)00112-5

Li, C., Jiang, B., Ju, W., Cheng, G., and Song, Y. (2019). Characteristics of tectonic deformation in the Daning-Jixian region, eastern Ordos Basin: implications for the exploration and development of coalbed methane. *Energy Explor. Exploitation* 37 (3), 907–921. doi:10.1177/0144598718816607

Li, G., and Zhang, H. (2020). Evolution history of coalbed methane reservoir and its difference in eastern Ordos Basin. *China Coalbed Methane* 17 (3), 3–8.

Li, S., Qian, M., and Shi, P. (2001). Permeability-strain equation relation to complete stress-strain path of coal sample. *Coal Geol. Explor.* 29 (1), 22–24. doi:10.3969/j.issn.1001-1986.2001.01.007

Li, S., Tang, D., Pan, Z., Xu, H., Tao, S., Liu, Y., et al. (2018). Geological conditions of deep coalbed methane in the eastern margin of the Ordos Basin, China: implications for coalbed methane development. *J. Nat. Gas Sci. Eng.* 53, 394–402. doi:10.1016/j.jngse.2018.03.016

Li, S., Tang, D. Z., Xu, H., and Yang, Z. (2012). Characteristics of coal reservoirs in Zhijin and Nayong regions, Guizhou province, China. *J. China Univ. Min. Technol.* 41 (6), 951–958.

Li, Z., Zhou, W., and Wu, Y. (2004). Generic analysis on the abnormal pressure of the gas reservoirs in the coal layers in China. *Mineralogy Petrology* 24 (4), 87–92. doi:10.19719/j.cnki.1001-6872.2004.04.016

Liu, C. (2006). Research on the earth temperature of surveying coal resources. *Coal Hebei* (3), 12–13. doi:10.3969/j.issn.1007-1083.2006.03.006

Liu, J. (2020). "*Sequence Stratigraphy and mineral resource Distribution in the late paleozoic cratonic Interior of western north China*,". Doctor (Beijing: China University of Mining and Technology).

Liu, J., Kang, Y., Chen, M., You, L., Zhang, T., Gao, X., et al. (2021). Investigation of enhancing coal permeability with high-temperature treatment. *Fuel* 290, 120082. doi:10.1016/j.fuel.2020.120082

Liu, Z., Zhu, W., Sun, Q., Jin, B., Xu, X., and Zhang, H. (2012). Characteristics of geotemperature-geopressure systems in petroliferous basins of China. *Acta Pet. Sin.* 33 (1), 1–17. doi:10.7623/syxb201201001

Lu, L., Qin, Y., and Guo, C. (2013). Modern geothermal field and coal seam heating temperature in Buzuo exploration area, Western Guizhou. *Coal Geol. China* 25 (10), 12–17. doi:10.3969/j.issn.1674-1803.2013.10.03

Meng, Z., Tian, Y., and Li, G. (2010). Characteristics of *in-situ* stress field in Southern Qinshui Basin and its research significance. *J. China Coal Soc.* 35 (6), 975–981. doi:10.13225/j.cnki.jccs.2010.06.014

Meng, Z., Zhang, J., and Wang, R. (2011). *In-situ* stress, pore pressure and stress-dependent permeability in the Southern Qinshui Basin. *Int. J. Rock Mech. Min. Sci.* 48 (1), 122–131. doi:10.1016/j.ijrmms.2010.10.003

Milkov, A. V., and Etiope, G. (2018). Revised genetic diagrams for natural gases based on a global dataset of> 20,000 samples. *Org. Geochem.* 125, 109–120. doi:10.1016/j.orggeochem.2018.09.002

Mukherjee, S., Rajabi, M., and Esterle, J. (2021). Relationship between coal composition, fracture abundance and initial reservoir permeability: a case study in the Walloon Coal Measures, Surat Basin, Australia. *Int. J. Coal Geol.* 240, 103726. doi:10.1016/j.coal.2021.103726

Mukherjee, S., Rajabi, M., Esterle, J., and Copley, J. (2020). Subsurface fractures, *in-situ* stress and permeability variations in the Walloon coal measures, eastern surat basin, queensland, Australia. *Int. J. Coal Geol.* 222, 103449. doi:10.1016/j.coal.2020.103449

Ministry of Natural Resources, PRC (2020). *Report on China oil and gas resource exploration and development in 2020*. http://gi.m.mnr.gov.cn/202109/t20210918_2681270.html. Beijing: Ministry of Natural Resources of the People's Republic of China.

Pan, Z., and Connell, L. D. (2011). Modelling of anisotropic coal swelling and its impact on permeability behaviour for primary and enhanced coalbed methane recovery. *Int. J. Coal Geol.* 85 (3-4), 257–267. doi:10.1016/j.coal.2010.12.003

Paul, S., and Chatterjee, R. (2011). Determination of *in-situ* stress direction from cleat orientation mapping for coal bed methane exploration in south-eastern part of Jharia coalfield, India. *Int. J. Coal Geol.* 87 (2), 87–96. doi:10.1016/j.coal.2011.05.003

Peng, T., Ren, Z., Wu, J., and Zhang, H. (2017). Distribution characteristics of the present-day geothermal field and its structural controls in deep part of panji mining area. *Geol. J. China Univ.* 23 (1), 157–164. doi:10.16108/j.issn1006-7493.2016161

Pu, Y., Li, S., Tang, D., and Chen, S. (2022). Effect of magmatic intrusion on *in situ* stress distribution in deep coal measure strata: a case study in linxing block, eastern margin of Ordos Basin, China. *Nat. Resour. Res.* 31 (5), 2919–2942. doi:10.1007/s11053-022-10099-8

Qin, Y., and Shen, J. (2016). Disccussion on the fundamental issues of deep coalbed methane geology. *Acta Pet. Sin.* 37 (1), 125–136. doi:10.7623/syxb201601013

Qin, Y., Shen, J., Wang, L., Yang, S., and Zhao, L. (2012). Accumulation effects and coupling relationship of deep coalbed methane. *Acta Pet. Sin.* 33 (1), 48–54. doi:10.7623/syxb201201006

Ranathunga, A. S., Perera, M. S. A., and Ranjith, P. (2014). Deep coal seams as a greener energy source: a review. *J. Geophys. Eng.* 11 (6), 063001. doi:10.1088/1742-2132/11/6/063001

Reisabadi, M. Z., Haghighi, M., Sayyafzadeh, M., and Khaksar, A. (2021). Stress distribution and permeability modelling in coalbed methane reservoirs by considering desorption radius expansion. *Fuel* 289, 119951. doi:10.1016/j.fuel.2020.119951

Salmachi, A., Rajabi, M., Wainman, C., Mackie, S., McCabe, P., Camac, B., et al. (2021). History, geology, *in situ* stress pattern, gas content and permeability of coal seam gas basins in Australia: a review. *Energies* 14 (9), 2651. doi:10.3390/en14092651

Shen, B., Shen, S., Wu, Q., Zhang, S., Zhang, B., Wang, X., et al. (2022). Carboniferous and permian integrative stratigraphy and timescale of north China block. *Sci. China Earth Sci.* 65 (6), 983–1011. doi:10.1007/s11430-021-9909-9

Song, Y., Liu, S., Ju, Y., Hong, F., Jiang, L., Ma, X., et al. (2013). Coupling between gas content and permeability controlling enrichment zones of high abundance coal bed methane. *Acta Pet. Sin.* 34 (3), 417–426. doi:10.7623/syxb201303001

Song, Y., Liu, S., Ma, H., Li, J., Ju, Y., Li, G., et al. (2016). Research on formation model and geological evaluation method of the middle to high coal rank coalbed methane enrichment and high production area. *Earth Sci. Front.* 23 (3), 1–9. doi:10.13745/j.esf.2016.03.001

Su, X., Liu, Y., Cui, Z., Zhang, J., Li, Y., and Wang, K. (2019). Influence of depressurization rate on gas production capacity of high-rank coal in the south of Qinshui Basin, China. *Petroleum Explor. Dev.* 46 (3), 642–650. doi:10.1016/s1876-3804(19)60044-3

Tan, J., Ju, Y., Hou, Q., Zhang, W., and Tan, Y. (2009). Distribution characteristics and influence factors of present geo-temperature field in Su-Lin mine area. *Huaibei Coalf.* 52 (3), 732–739.

Wang, G., Qin, Y., Shen, J., Chen, S., Han, B., and Zhou, X. (2018). Dynamic-change laws of the porosity and permeability of low-to medium-rank coals under heating and pressurization treatments in the eastern junggar basin, China. *J. Earth Sci.* 29, 607–615. doi:10.1007/s12583-017-0908-4

Wang, X., Zhang, Q., Wang, L., Ge, R., and Chen, J. (2010). Structural features and tectonic stress fields of the Mesozoic and Cenozoic in the eastern margin of the Ordos basin, China. *Geol. Bull.* 29 (8), 1168–1176. doi:10.3969/j.issn.1671-2552.2010.08.009

Ward, C. R. (2016). Analysis, origin and significance of mineral matter in coal: an updated review. *Int. J. Coal Geol.* 165, 1–27. doi:10.1016/j.coal.2016.07.014

Weniger, S., Weniger, P., and Littke, R. (2016). Characterizing coal cleats from optical measurements for CBM evaluation. *Int. J. Coal Geol.* 154, 176–192. doi:10.1016/j.coal.2015.12.005

Wu, C., Qin, Y., and Fu, X. (2007). Elastic energy of coal reservoir and its controlling effect on coalbed methane accumulation. *Sci. China (D)* 37 (9), 1163–1168. doi:10.3969/j.issn.1674-7240.2007.09.003

Wu, S., Peng, T., and Guo, Y. (2013). Ground temperature distribution pattern and its abnormal factor analysis in qianyingzi coalmine, northern anhui. *Coal Geol. China* 25 (6), 30–35. doi:10.3969/j.issn.1674-1803.2013.06.007

Wu, S., Tang, D., Li, S., Wu, H., Hu, X., and Zhu, X. (2017). Effects of geological pressure and temperature on permeability behaviors of middle-low volatile bituminous coals in eastern Ordos Basin, China. *J. Petroleum Sci. Eng.* 153, 372–384. doi:10.1016/j.petrol.2017.03.034

Xiao, Y., Liu, D., Kong, X., and Lian, D. (2009). Analysis of No.9 coal geotemperature characteristics and impacting factors in longfeng minefield. *Coal Geol. China* 21 (1), 45–47. doi:10.3969/j.issn.1674-1803.2009.01.013

Xu, F., Yan, X., Lin, Z., Li, S., Xiong, X., Yan, D., et al. (2022). Research progress and development direction of key technologies for efficient coalbed methane development in China. *Coal Geol. Explor.* 50 (3), 1–14. doi:10.3969/j.issn.1001-1986.2022.03.001

Xu, H., Sang, S., Yang, J., Jin, J., Hu, Y., Liu, H., et al. (2016). *In-situ* stress measurements by hydraulic fracturing and its implication on coalbed methane development in Western Guizhou, SW China. *J. Unconv. Oil Gas Resour.* 15, 1–10. doi:10.1016/j.juogr.2016.04.001

Xu, H., Tang, D., Tang, S., Zhang, W., Zhang, S., Tao, S., et al. (2010). Coal reservoir characteristics and prospective areas for Jurissic CBM exploitation in western Ordos basin. *Coal Geol. Explor.* 38 (1), 26–28+ 32. doi:10.3969/j.issn.1001-1986.2010.01.006

Yan, X., Xu, F., Nie, Z., and Kang, Y. (2021). Microstructure characteristics of Daji area in east Ordos Basin and its control over the high yield dessert of CBM. *J. China Coal Soc.* 46 (8), 2426–2439. doi:10.13225/j.cnki.jccs.CB21.0751

Yang, S., Cui, F., Yang, S., and Zhang, S. (2005a). Experimental study on mechanism of gas flow in coal bed. *China Coalbed Methane* 2 (1), 36–39. doi:10.3969/j.issn.1672-3074.2005.01.009

Yang, S., Xiao, C., Wang, X., and Yang, Q. (2005b). Stress sensitivity of rock and its influence on productivity for gas reservoirs with abnormal high pressure. *Nat. Gas. Ind.* 25 (5), 94–95. doi:10.3321/j.issn:1000-0976.2005.05.030

Yang, X. (2015). Characteristics of CBM reservoir in Huangling-Longxian coalfield. *Coal Geol. Explor.* 43 (4), 41–45. doi:10.3969/j.issn.1001-1986.2015.04.009

Yang, X., Xu, F., Wang, H., Li, S., Lin, W., Wang, W., et al. (2022). Exploration and development process of coalbed methane in eastern margin of Ordos Basin and its enlightenment. *Coal Geol. Explor.* 50 (3), 5. doi:10.3969/j.issn.1001-1986.2022.03.004

Yang, X., and Zhang, Y. (2008). Experimental study of effect of temperature on coal gas permeability under gas-solid coupling. *J. Geomechanics* 14 (4), 374–380. doi:10.3969/j.issn.1006-6616.2008.04.007

Yuan, Y., Zhu, W., Mi, L., Zhang, G., Hu, S., and He, L. (2009). "Uniform geothermal gradient" and heat flow in the qiongdongnan and pearl river mouth basins of the south China sea. *Mar. Petroleum Geol.* 26 (7), 1152–1162. doi:10.1016/j.marpetgeo.2008.08.008

Zhang, L. (2012). Geotemperature characteristics and impacts from geological factors in Shunhexi Mine Area. *Coal Geol. China* 24 (7), 29–33. doi:10.3969/j.issn.1674-1803.2012.07.07

Zhang, Y., Li, S., Tang, D., Liu, J., Lin, W., Feng, X., et al. (2022). Geological and engineering controls on the differential productivity of CBM wells in the Linfen block, southeastern Ordos Basin, China: insights from geochemical analysis. *J. Petroleum Sci. Eng.* 211, 110159. doi:10.1016/j.petrol.2022.110159

Zhang, Y., Li, S., Tang, D., Zhao, X., Zhu, S., and Ye, J. (2020). Structure-and hydrology-controlled isotopic coupling and heterogeneity of coalbed gases and co-produced water in the Yanchuannan block, southeastern Ordos Basin. *Int. J. Coal Geol.* 232, 103626. doi:10.1016/j.coal.2020.103626

Zhang, Y., and Tang, S. (2001). Research on coal reservoir pressure of some mine areas in north China. *Acta Geosci. Sin.* 22 (2), 165–168. doi:10.3321/j.issn:1006-3021.2001.02.014

Zhang, Z., Zhang, R., Wu, S., Deng, J., Zhang, Z., and Xie, J. (2019). The stress sensitivity and porosity sensitivity of coal permeability at different depths: a case study in the Pingdingshan mining area. *Rock Mech. Rock Eng.* 52 (5), 1539–1563. doi:10.1007/s00603-018-1633-8

Zhao, D., Chen, Z., Cai, X., and Li, S. (2007). Analysis of distribution rule of geostress in China. *Chin. J. Rock Mech. Eng.* 26 (6), 1265–1271. doi:10.3321/j.issn:1000-6915.2007.06.024

Zhao, J., Tang, D., Lin, W., Qin, Y., and Xu, H. (2019). *In-situ* stress distribution and its influence on the coal reservoir permeability in the Hancheng area, eastern margin of the Ordos Basin, China. *J. Nat. Gas Sci. Eng.* 61, 119–132. doi:10.1016/j.jngse.2018.09.002

Zhao, J., Tang, D., Xu, H., Li, Y., Li, S., Tao, S., et al. (2016). Characteristic of *in situ* stress and its control on the coalbed methane reservoir permeability in the eastern margin of the Ordos Basin, China. *Rock Mech. Rock Eng.* 49 (8), 3307–3322. doi:10.1007/s00603-016-0969-1

Zhao, X., Tang, D., and Zhang, Y. (2021). Establishment and optimization of drainage system for deep coalbed methane in south Yanchuan CBM field. *Coal Sci. Technol.* 49 (6), 251–257. doi:10.13199/j.cnki.cst.2021.06.030

Zhong, L. (2003). Pressure characteristics of coal reservoirs in China. *Nat. Gas. Ind.* 23 (5), 132–134. doi:10.3321/j.issn:1000-0976.2003.05.043

Zhu, H., and Tao, Z. (1994). Distribution of geostress in different rocks. *Acta Seismol. Sin.* 16 (1), 49–63.

Zhu, Q., Lu, X., and Yang, Y. (2019). Coupled activation technology for low-efficiency productivity zones of high-rank coalbed methane in Zhengzhuang block, Shanxi. *China* 44 (8), 2547–2555. doi:10.13225/j.cnki.jccs.KJ19.0428

Zoback, M., Barton, C., Brudy, M., Castillo, D., Finkbeiner, T., Grollimund, B., et al. (2003). Determination of stress orientation and magnitude in deep wells. *Int. J. Rock Mech. Min. Sci.* 40 (7-8), 1049–1076. doi:10.1016/j.ijrmms.2003.07.001